International Information and Engineering Technology Association
Advancing the World of Information and Engineering

Traitement du Signal
Vol. 40, No. 5, October, 2023, pp. 2215-2223
Journal homepage: http://iieta.org/journals/ts

Enhanced Classification of Alzheimer's Disease Stages via Weighted Optimized Deep Neural Networks and MRI Image Analysis

Mudiyala Aparna, Battula Srinivasa Rao*

School of Computer Science and Engineering, VIT-AP University, Andhra Pradesh 522237, India

Corresponding Author Email: srinivas.battula@vitap.ac.in

https://doi.org/10.18280/ts.400538

Received: 2 January 2023
Revised: 28 March 2023
Accepted: 16 May 2023
Available online: 30 October 2023

Keywords:
image processing techniques, Alzheimer's data, optimization techniques, deep learning models, transfer learning techniques

ABSTRACT

Alzheimer's disease, a debilitating neurological disorder, precipitates irreversible cognitive decline and memory loss, predominantly affecting individuals aged 65 years and above. The need for an automated system capable of accurately diagnosing and stratifying Alzheimer's disease into distinct stages is paramount for early intervention and management. However, existing deep learning methodologies are often hampered by protracted training times. In this study, a time-efficient approach incorporating a two-phase transfer learning technique is proposed to surmount this challenge. This method is particularly efficacious in the analysis of Magnetic Resonance Imaging (MRI) data for the identification of Alzheimer's disease. The proposed detection system employs two-phase transfer learning, augmented with fine-tuning for multi-class classification of brain MRI scans. This allows for the categorization of images into four distinct classes: Mild Dementia (MD), Moderate Dementia (MOD), Non-Dementia (ND), and Very Mild Dementia (VMD). The classification of Alzheimer's disease was conducted using various pre-trained deep learning models, including ResNet50V2, InceptionResNetV2, Xception, DenseNet121, VGG16, and MobileNetV2. Among the models tested, ResNet50V2 demonstrated superior performance, achieving a training classification accuracy of 99.35% and a testing accuracy of 99.25%. The results underscore the potential of the proposed method in delivering more accurate classifications than those obtained from extant models, thereby contributing to the early detection and stratification of Alzheimer's disease.

1. INTRODUCTION

Alzheimer's disease, a neurological disorder characterized by a gradual deterioration of memory, cognition, and basic task performance ability, predominantly afflicts individuals aged 65 and above. As the most prevalent cause of dementia in the nation, it currently ranks as the seventh leading cause of death [1]. The deterioration of brain tissues, culminating in neuronal death, precipitates memory loss and adversely impacts daily task performance, including reading, speaking, and writing. However, early diagnosis and intervention can enhance patients' quality of life [2-5].

The onset of symptoms is typically insidious, gradually exacerbating the patient's health condition over time. Predictive models project that by the year 2050, one in 85 individuals will be diagnosed with Alzheimer's disease, signifying a substantial annual case increase [6-8]. Approximately 60–80% of diagnosed cases progress to advanced stages of the disease.

The Global Deterioration Scale (GDS) is frequently employed for dementia assessment, while the Clinical Dementia Rating (CDR) scale aids in understanding and communication with dementia patients [9-11]. Characteristic brain changes in Alzheimer's disease include enlarged ventricles and a reduction in the size of the cerebral cortex and hippocampus. The latter, when reduced, impairs both spatial and episodic memory. The neuronal damage that results contributes to difficulties in planning, judgement, and short-term memory. The ongoing cell degeneration further impairs synapses and neuronal terminals.

Numerous investigations have focused on the categorization and early detection of Alzheimer's disease. Brain Magnetic Resonance Imaging (MRI) analysis is a common and effective method for disease identification. These MRI images are reviewed by medical professionals to detect the presence of abnormalities such as tumors, tissue changes, or degenerative conditions. The integration of deep learning and machine learning models with various medical imaging modalities, including mammography, ultrasound, and MRI, has been explored [12, 13]. These models have demonstrated significant results in disease classification and detection across various domains, including cardiovascular, pulmonary, neural, retinal, mammary, and skeletal diseases.

In the present study, the utility of transfer learning is demonstrated in achieving accurate Alzheimer's disease diagnosis using two pre-trained base models. Existing diagnostic tests in neurology clinics are swift, cost-effective, and can identify Alzheimer's disease with accuracy exceeding 95%. However, comprehensive testing in most hospitals and clinics only achieves a 70% accuracy rate.

This study's focus is on the nucleus accumbens, an integral brain region involved in motivation processing. This region within the ventral striatum is often overlooked in Alzheimer's research, primarily examined in studies focusing on emotional and motivational processes. A deep learning network was employed in this study to classify and identify Alzheimer's disease using an MRI dataset.

The remainder of the paper is organized as follows: Section 2 provides a literature review of previous works. Section 3 discusses the dataset, proposed methods, and pre-trained models with two-phase Transfer Learning. Section 4 presents the results and accompanying discussion, including a comparison with different deep learning models. Figure 1 depicted the various stages of MRI images.

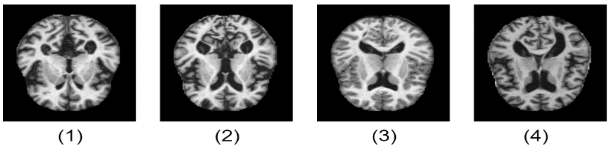

Figure 1. Examples of MRI images illustrating various stages of AD (1) Mild demented (2) Moderate demented (3) Non-demented (4) Very mild demented

2. LITERATURE SURVEY

In recent years AD detection has garnered increasing academic interest, suggesting ML and DL as common approaches for automatic detection. With reference to the same, the current study used the DL methodology for AD detection. Hence, the scope of this study is limited to DL approaches and DL models in the literature.

El-Dahshan et al. [14] used a three-step hybrid approach including feature extraction, dimensionality reduction, and classification for developing a disease diagnosis. The first step was to acquire MRI-related data, then using the Principal Component Analysis (PCA) to reduce image features, and finally to create two different classifiers. One classifier was constructed using a feed-forward neural network, while other was constructed using the k-nearest neighbour technique. This classification had the benefit of being quick, simple, affordable, and non-invasive to operate.

In their research, Ahmed et al. [15] used a patch-based classifier and a CNN-based model for Alzheimer's disease diagnosis. The results showed that the processing costs were reduced and disease identification was significantly improved. Using algorithms based on deep learning, they extracted features directly from the input after performing various operations on the data set. To enhance the ability to represent characteristics in MRI scans, these models were built on multi-layered algorithms and hierarchical architectures.

In research conducted by Hong et al. [13] LSTM (long short-term memory) recurrent neural networks were used for disease prediction. The cells, the post-fully linked layers, and the pre-fully connected layers were the three layers that were utilised in this method. The levels of this method primarily made use of time series data. They made remarks about the disease's outlook rather than describing the condition itself.

Further, Islam et al. [16] used a deep convolutional network for disease detection, and they used the Inception-V4 network to train it. The input and output of these layers were handled using a number of filter concatenation methods in the Inception-A,B,C and Reduction-A,B modules. They were trained and tested using the Open-Access Imaging Studies (OASIS) dataset and improved their overall accuracy to 73.75 percent.

For diagnosing Alzheimer's disease using longitudinal structural MRI images, Zhang et al. [17] built a benchmark feature extraction technique for databases.

A feature extraction algorithm based on significant inter-subject variability was developed by Guerrero et al. [18] The regions of interest (ROI) for variable selection were identified with the help of a sparse regression model. Due to the binary classification, their proposed model only achieves an overall accuracy of 71%.

Ahmed et al. [19] developed a model in which the texture was combined with a hybrid feature vector that considered the hippocampus's shape and cortical thickness. The authors classified the MRI scan feature vectors using the linear discriminant analysis (LDA) classification algorithm. The overall accuracy for the proposed method was 62.7%, and the dataset used to evaluate it was obtained from the Alzheimer's Disease Neuroimaging Initiative (ADNI). Previous research has demonstrated that adults with Alzheimer's disease have smaller brain volumes in the cortical and hippocampal regions as well as the nucleus accumbens.

3. MATERIALS AND METHODS

3.1 Data set description

The ADNI Database was used by the researchers in this study. The MRI scans in this database were classified as mildly demented, non-demented, very mildly demented, and moderate demented [20-22]. All images were in the Portable Network Graphics (PNG) file type and had a resolution of 224 × 224 pixels. Three channels with repeating RGB values built up the images, which were grayscale. The target dataset was obtained from an open ADNI Repository. This dataset contained MRI scans of people with Mild Demented, Non-Demented, Very Mild Demented, and Moderate Demented. An image dataset that included images from different phases of AD was used to train the suggested model [23-26]. We trained the proposed model using an image dataset containing images from various stages of AD. In our dataset we have total 20,926 MRI images and splited for training and testing like 14,648 images for traing and 6278 images for testing in percentages 70% of data for training and 30% of data for testing. Table 1 displays the total number of input image samples for each class.

Table 1. Split four classes of MRI image datasets for training and testing

Train/Test	Classification	No. of Images	Total	Percentage (%)
For Training	non-Demented	**3788**		
	very Mild-Demented	**3700**	**14,648**	**70%**
	mild-Demented	**3600**		
	moderate-Demented	**3560**		
For Testing	non-Demented	**1629**		
	very Mild-Demented	**1600**	**6278**	**30%**
	mild-Demented	**1569**		
	moderate-Demented	**1480**		
Total			**20,926**	

3.2 Proposed methodology

The pre-processing layer receives MRI scans from various sources. Thereafter the pre-processing layer alters the image's dimensions. This model recognises AD and categorise it into four classes. Figure 2 shows the number of images graphically.

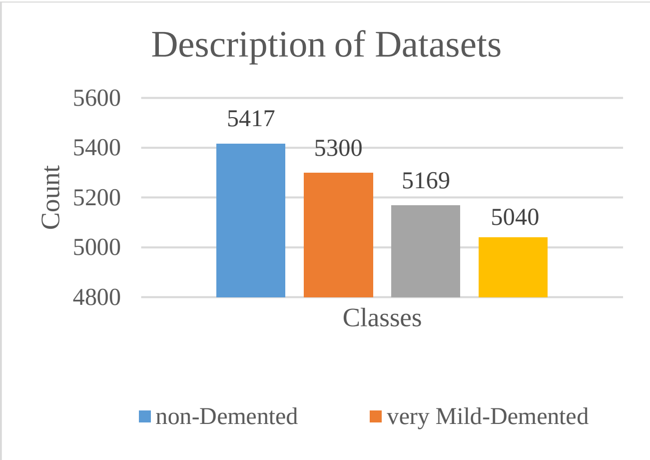

Figure 2. Graphical representation of Alzheimer's datasets

The proposed deep learning-based system model employed magnetic resonance imaging (MRI) data for early disease identification and categorization. It was divided into two layers: pre-processing and application. Training data, including MRI images, were acquired in raw format. Raw data were processed by a pre-processing layer that transformed the image to 224×224×3 dimensions. ResNet50V2, InceptionResNetV2, Xception, DenseNet121, VGG16, and MobileNetV2 pre-trained models were modified for transfer learning in the second layer, which is the Application layer. In the proposed study, a deep learning-based network was deployed with pre-trained models to detect and categorise Alzheimer's disease through a two-phase transfer learning process. Figure 3 provides a detailed description of the proposed model.

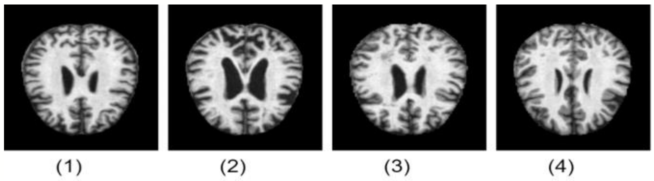

Figure 3. MRI images after pre-processing. (1) Mild demented (2) Moderate demented (3) Non-demented (4) Very mild demented

3.3 Classification using two-phase transfer learning

For a 4-way classification of AD, the suggested method made use of the two-phase transfer learning technique. Figure 4 depicts the architecture for implementing two-phase transfer learning.

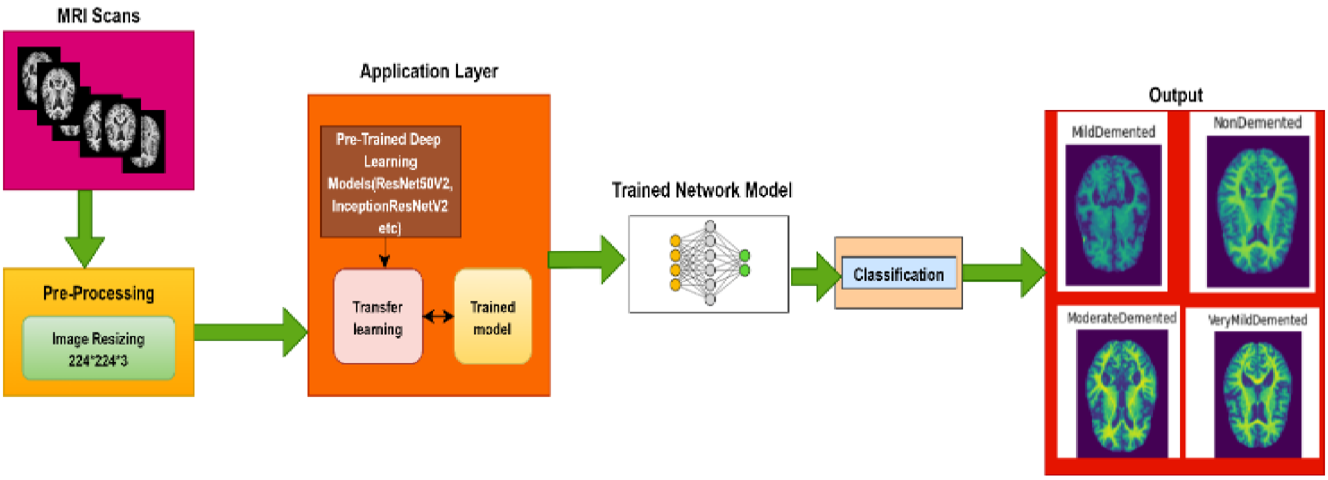

Figure 4. Basic architecture of proposed methodology

The transfer learning method can be utilized when we have a large set of training data for parameter learning. When learning a new task, we start with a trained network like Resnet50v2. The Resnet50v2 model, which had previously been trained on ImageNet, was applied to an MR image of the brain from the ADNI dataset. The outputs of these 1000 categories were the results of these frozen fully-connected layers, which needed the use of the two-phase transfer learning approach. A new fully-connected layer, a SoftMax layer, and an output layer for four-class classification were required to replace them [27-33]. The network was then given a training set of MR images as well as training options. The model's accuracy was then evaluated. To calculate the loss percentage, The output size depended on the number of classes, and the Cross-Entropy function was used the domain D was made up of two parts: Y denotes the Feature Space, and P(Y) denotes associated marginal probability. In P(Y),Y={y_1,y_2,.....y_n} The number of input images was denoted by n. In the mathematical equation, the domain was denoted by

$$Domain = \{Y, P(y)\} \quad (1)$$

Marginal probability and associated feature space for two separate domains were different. Label space Z and objective prediction function *f(.)* were also used to express a task T in domain D.

$$Task = \{Z, f(.)\} \quad (2)$$

The training procedure of the features educates the prediction function *f (.)*, which was then applied to estimate the testing data. One target domain $Domain_t$, and one source domain $Domain_s$, were both present in the suggested paradigm. The source data occurrence with the label z_{si} was initialised as the y_{si}, and the target data occurrence with the label z_{ti} was initialised as the y_{ti}.

The following can be written about the target domain and the source domain:

$$Domain_t = \{(y_{t1}, z_{t1}), (y_{t2,} z_{t2}), \dots (y_{tn,} z_{tn})\} \quad (3)$$

$$Domain_s = \{(y_{s1}, z_{s1}), (y_{s2,} z_{s2}), \dots (y_{sn,} z_{sn})\} \quad (4)$$

Transfer learning is the most common way of learning a predictive function *f (.)*. It trains the objective space utilizing the information accumulated for the source activities and source domain. The predictive function *f (.)* predicts the label of new occurrence *(y)*. *f(y)* is mathematically represented as $f(y) = P(Z/_Y)$.

Algorithm:

- **Input**
  - P(Y),Y={y_1,y_2,.....y_n} no. of samples in dataset
- **Pre-Training**
  - **for** length of samples **do**
    - Pre-Trained Network from Source Domain (D_s)
    - Training set in Target Domain (D_t)
    - Validation set in Target Domain (D_t)
    - Training/Validate Samples
  - **end for**
- **Fine-Tuning**
  - **For** $f(y)$ length of features **do**
    - Fine-tuning Specific layers of pre-trained model $\{Y, P(y)\}$
    - Fine-tuning the pre-trained model on training Dataset (D_t)
    - Deploy the fine-tuned model on Test Dataset (D_t)
  - **end for**
- **Output**
  - Categorized Images from Test Dataset.

3.4 Pre-trained models with two-phase transfer learning

3.4.1 VGG16

The VGG16 model has 13 convolutional layers, 2 fully connected layers, and 1 SoftMax layer that uses convolutions and fully connected layers to classify data. A 16-layer network was created by Karen and Andrew. The Basic model only has 3×3 convolutional layers. In the first and second convolutional layers, 64 feature kernel filters of size 3×3 were used. An RGB image of depth 3 was sent through the first and second convolutional layers, where its dimensions were transformed into 224×224×64. The output was then passed to the maximum pooling layer with a stride of 2. Third and fourth convolutional layers utilise a 124-feature kernel filter with a filter size of 3×3. Following these two layers, we added a max pooling layer with stride 2, resulting in a final dimension of 56×56×128. Convolutional layers with a 3×3 kernel size made up the fifth, sixth, and seventh levels. The basis for each of them was a set of 256 feature maps. After these layers came a max pooling layer with a stride of 2. Two groups of 3×3 convolutional layers were located at locations 8 through 13. All these sets of convolutional layers use 512-bit kernel filters. When these were been completed, a max pooling layer with a stride of 1 was be added. Then the fourteenth and fifteenth levels were completely connected, 4096-unit hidden layers that came after the output SoftMax layer. In the last five layers of this model, we classified Alzheimer's disease using transfer learning.

3.4.2 Densenet121

The DesneNet121 model is made up of five convolutional blocks. The Convolved image was sent to Conv2 size 56×56 from the max pooling block, the initial convolution block (Block-1) processes the image to fit Conv1 size 112×112.Following the transfer of the obtained features to the dense layer, the output (Block 2), Conv 3 for 28×28, Conv 4 for 14×14, and Conv 5 for 7×7 were obtained. Convolutional CNNs frequently calculated the output layers (lth) by applying a non-linear transformation H l (.) to the output of the preceding layer X_ (l-1).

$$X_l = H_l(X_{l-1}) \quad (5)$$

The layer output functionality maps and the inputs are concatenated by DenseNets instead of being truly added together. DenseNet, can easily improve information flow across layers by using a simple Convolutional model, The features of all earlier layers provide input to the layer below: Following that, the equation is:

$$X_l = H_l([X_0, X_1, X_2 \dots X_{l-1}]) \quad (6)$$

where, [X_0, X_1, X_2,…, X_{l-1},] is created by joining the output maps of earlier layers into a single tensor. Out of the functions, H_l(.) represents a non-linear transformation function. There are three main operations in this function: Batch normalisation (BN), activation function (ReLU), and convolution (CONV). In this architecture the growth rate k aided in the following generalisation of the l^{th} layer:

$$K^{(l)} = (K^{[0]} + K(l-1)) \quad (7)$$

where, $K^{[0]}$ is known as the number of channels.

3.4.3 MobilenetV2

In MobileNetV2, two distinct block types can be seen. The first is a residual block with a stride of one. Another way to reduce is with a two-stride block. There are three levels that separate the two kinds of blocks. This time around, the convolution that took place in the first layer was a simple 1x1 one that used ReLU6, whereas the convolution that took place in the second layer was more involved. Another 1×1 convolution without nonlinearity made up the third layer. When used again, ReLU was said to limit the power of deep networks to a linear classifier, at least for non-zero volume output domain regions. There were 155 layers total in MobileNetv2, including a categorization layer. This model comprises of 154 pretrained network layers (convolutional basis) and 2 additional layers. The pre-trained model will lose its learned information if all 156 layers are trained since the classifier's random weights will cause very large gradient updates. By freezing the convolutional basis during training, weight updates are stopped. The pretrained model's layers are all frozen by setting the trainable flag of the entire model to false.

3.4.4 Xception

The Xception model, which is composed of depth-wise separable convolution layers, was broken down into three fundamental sections: the input flow, the middle flow, and the exit flow. The Xception model first recognised three flows in the visual data: the input flow, the middle flow, which occurred eight times total, and the exit flow. The batch normalisation method was applied to each convolutional layer, as well as each layer that had the potential to be subdivided into a smaller number of layers. The network's feature extraction was based on the model's 36 convolutional layers. The top-1 accuracy of the Xception model for four classes was 79% then trained on 299 x 299 ImageNet images. The design of a regression model with only one class as the output requires the usage of a pretrained Xception ImageNet model. Before introducing a max pooling layer, the Xception model's last completely linked layer was removed. In addition to this, the output layer was enlarged to incorporate a dense layer composed of a single neuron with a linear activation function. The model was trained over 50 iterations using an Adam optimization approach with a learning rate of 0.001. The image dataset was divided into 16 micro batches to facilitate training. The four groups were classified using MRI images using a distinct pretrained Xception model.

3.4.5 InceptionResNetV2

Residual Inception Block is the fundamental unit of Inception-ResNet-V2. Following each block is a 1×1 convolution filter expansion layer, which scales the dimensionality prior to addition to match the depth of the input. Only the traditional levels of this architecture utilise batch normalisation. The image input size for Inception-ResNet-V2 is 299×299, and there are 164 layers in total. The Residual Inception Block employs convolutional filters of various sizes and residual connections. In order to address the problem of deep network degradation and accelerate training, this design makes advantage of residual connections.

Max Pooling was implemented instead of Flatten after this core design to minimise overfitting in the convolutional structure naturally because there were no parameters to be tuned and by strengthening the connection between the feature importance and label category. Due to this, max Pooling is also more parameter-efficient than the Flatten technique. According to Szegedy, Ioffe, Vanhoucke, and Alemi Addition of a Dropout layer with a fixed value of 0.8 is made.

$$\sigma(x)_i = \frac{e^{x_i}}{\sum_{j=1}^{k} e^{y_i}} \tag{8}$$

The dense layer was activated using the SoftMax activation function, as shown in Eq. (3), where x and y represent input and output, K represented the number of classes, and e represented the common exponential function, which in this instance is e = 2.718.

$$w' = w - \alpha \times \nabla(w; x^{(i)}; y^{(i)}) \tag{9}$$

The iterative Stochastic Gradient Descent (SGD) technique was used for optimization during backpropagation. Its formula is given in Eq. (4), where w stands for weight, α for learning rate, and $\nabla\left(w; x^{(i)}; y^{(i)}\right)$ for the gradient to weight, input, and output/label, respectively.

3.4.6 Proposed ResNet50V2 with 2PTL

ResNet50v2 is one of the well-known models that excels in solving a variety of computer vision issues.

Some of the models are VGG16, DenseNet121, Xception, MobileNetV2, InceptionResNetV2. These models are developed using a huge quantity of data from many different image categories. These trained model weights can be used by transfer learning algorithms to solve a variety of computer vision problems with a constrained number of datasets and computing resources. This study made use of a sizable dataset of medical image data, and we carried out transfer learning with ten distinct pre-trained weights derived from the ResNet50v2 model. The ResNet50v2 Two Phase Transfer Learning model's architecture and its 10 various pre-trained weights are covered in the sections that follow. A CNN model called the ResNet50v2 model has 50 layers. Figure 5 depicts the architecture of Proposed ResNet50v2 model, as well as its fine-tuning setup for ResNet50v2 Transfer Learning.

Also, the architecture for proposed fine-tuned ResNet50v2 Two-Phase Transfer Learning presented in Table 2.

Table 2. Description of Resnet50v2 two-phase transfer learning

Layers	Output Size	Layer
Conv1	112 × 112	7 × 7, 64, Stride 2
Conv2_x	56 × 56	3 × 3 Maxpooling, Stride=2 [1 × 1, 64 3 × 3, 64 1 × 1, 256] × 3
Conv3_x	28 × 28	[1 × 1, 128 3 × 3, 128 1 × 1, 512] × 4
Conv4_x	14 × 14	[1 × 1, 256 3×3,256 1 × 1, 1024] ×6
Conv5_x	7 × 7	[1 × 1, 512 3 × 3, 512 1 × 1, 2048] × 3
fully connected layer_1	1 × 1	max pooling Features-in=2048, Features-out=2048
fully connected layer _c2	1 × 1	dropout= 0.5
fully connected layer_c3	1 × 1	Features-in=2048, Features-out=2048 Relu, dropout=0.5 Features-in=2048, Features-out=2

A number of convolutional layers make up the ResNet50v2 design. The first convolutional layer has 64 distinct kernels, a stride size of 2, and a filter size of 7 × 7. Then up to 3 × 3 pooling with a step size of 2 is used. Three layers of convolution (1 × 1,64 kernel), (3 × 3,64 kernel) and (1 × 1,256 kernel) exist in the next convolution, each repeated three times. The same procedure was followed for each of three convolutional layers (1 × 1,128 kernels), (3 × 3,128 kernels) and (1 × 1,512 kernels), three convolutional layers (1 × 1,256 kernels), (3 × 3,256 kernels) Repeated 4 times and (1 × 1,1024 kernel) for 6 iterations each, and 3 layers of convolution (1 × 1,512 kernel), (3 × 3,512 kernel) and (1 × 1,2048 kernel) for 3 iterations each. It is followed by Max pooling (max pool). A convolution layer, batch normalization, and ReLU are frequently used in combined with hidden layers. The original ResNet50v2 model ends with a fully connected (fc) layer that has 1000 out-features (for 1000 class). To enhance the ResNet50v2 model, a group of fully connected layers replaces this one. When a dropout occurs, the first similar feature layer is chosen (with 2048 out features) and the chance of using that layer is set to 0.5. The second fc layer is then followed by a ReLU and dropout layer with a probability of 0.5. For four-class classification, the final FC layer only has 4 out-features and 2048 in-features. i.e., mild demented, moderate demented, very mild demented, non demented. In this study, we evaluated transfer learning using 10 different ResNet50v2 model pre-trained weights. Several datasets were used to construct these pre-trained weights. These datasets had a several variations, as we were dealing with medical image datasets. Figure 6 depicts the modified Resnet50v2 with 2 phase transfer learning.

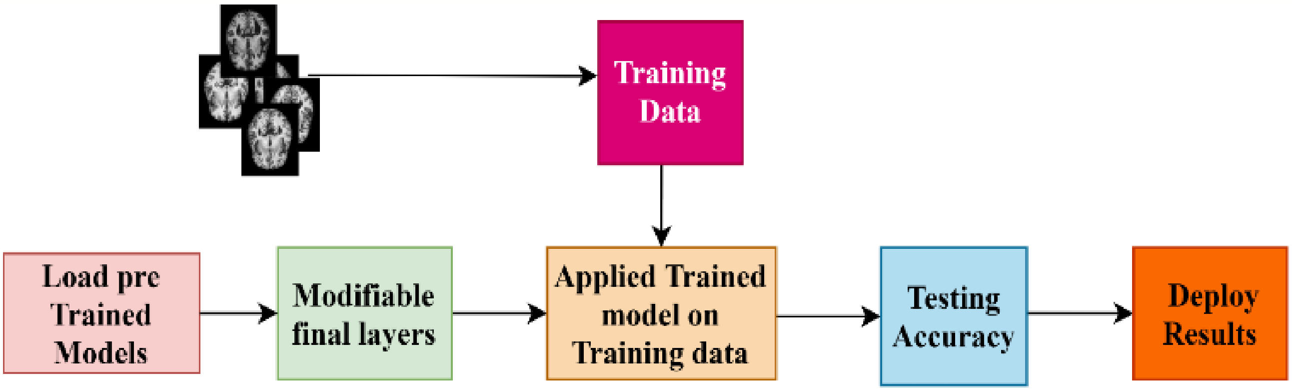

Figure 5. Basic architecture deployment overview

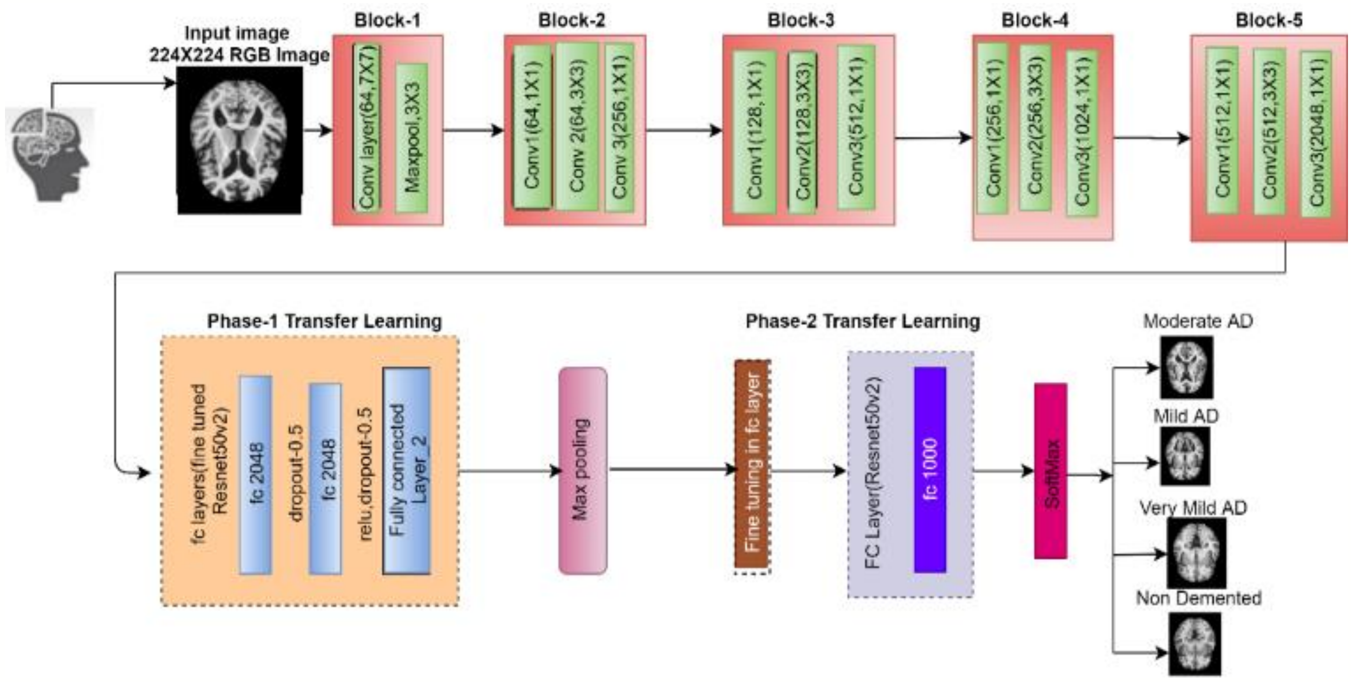

Figure 6. Architecture of proposed model modified ResNet50V2 with 2PTL

4. RESULTS

The model for classifying data was developed using TensorFlow, a programme that supported transfer learning. Stochastic gradient descent with momentum (SGDM) was utilised as the optimizer to determine the weight and bias variables, minimise the loss function, and decrease the loss function during the training of 20,926 images. There 50 were epochs utilised, a small batch size of 512, a learning rate of 0.0001, and an early stopping parameter of 4 for the validation Testing. The number of iterations needed to finish 1 epoch in our case was 107. Over-fitting can be minimized by evaluating the model's reliability after a validation test or by adding an extra epoch to the data set. Since accuracy is the key evaluation parameter, the impact of changing the learning rate from 1e-2 to 1e-5 on the training and testing accuracy of the model was examined. Even though the model's best output was obtained at a learning rate of 1e-4, that rate was still substantially faster than the average. We used a learning rate of 1e-4 to test every model. The performance of a classification model can be evaluated using the confusion matrix, which was used to measure precision. In this study, we examined 6 different models with the same data. An Alzheimer's disease detection model was used to assess the quality of an MRI scan. The total number of images in the dataset were 20,926, four categories, and each class had 5,231 images. This ensured that all classes were represented equally in the dataset. Using 50 epochs of data, the network was trained from basics. Data from each experiment consisted 30% of test data and 70% of training data. Different evaluation criteria might be used to assess the outcomes. Table 3 represented confusion matrix for DenseNet121. Table 4 and Table 5 generated confusion matrix on testing for MobileNetV2 and VGG16.

$$sensitivity = \frac{\left(D_p / N_p \right)}{\left(D_p / N_p \right) + \left(D_n / N_n \right)} * 100 \tag{10}$$

$$specificity = \frac{\left(D_m / N_n \right)}{\left(D_m / N_m \right) + \left(D_e / N_e \right)} * 100 \tag{11}$$

$$precision = \frac{\left(D_p / N_p \right)}{\left(D_p / N_p \right) + \left(D_e / N_e \right)} * 100 \tag{12}$$

$$accuracy = \frac{\left(D_P / N_p \right) + \left(D_m / N_m \right)}{p + m} * 100 \tag{13}$$

$$missrate = 1 - \frac{\left(D_P / N_p \right) + \left(D_m / N_m \right)}{p + m} * 100 \tag{14}$$

$$falsepositive\, rate = 1 - \frac{\left(D_m / N_n \right)}{\left(D_m / N_m \right) + \left(D_e / N_e \right)} * 100 \tag{15}$$

$$falsenegative\, rate = 1 - \frac{\left(D_p / N_p \right)}{\left(D_p / N_p \right) + \left(D_n / N_n \right)} * 100 \tag{16}$$

Table 3. Confusion matrix generated by testing DenseNet121

Class Label	ND	VMD	MD	MOD	Total Data	Accuracy
ND	1399	45	109	76	1629	85.88
VMD	126	1289	75	110	1600	80.05
MD	20	35	1482	32	1569	91.43
MOD	32	42	40	1366	1480	92.29

Table 4. Confusion matrix generated by testing MobileNetV2

Class Label	ND	VMD	MD	MOD	Total Data	Accuracy
ND	1465	45	59	60	1629	89.93
VMD	127	1365	48	60	1600	85.31
MD	20	15	1511	23	1569	96.30
MOD	15	22	18	1425	1480	96.29

Table 5. Confusion matrix generated by testing VGG16

Class Label	ND	VMD	MD	MOD	Total Data	Accuracy
ND	1465	45	59	60	1629	89.93
VMD	77	1465	23	35	1600	91.05
MD	12	10	1536	11	1569	97.80
MOD	15	22	18	1425	1480	96.29

Table 6. Confusion matrix generated by testing Xception

Class Label	ND	VMD	MD	MOD	Total Data	Accuracy
ND	1479	45	39	66	1629	90.79
VMD	26	1489	55	30	1600	93.06
MD	20	25	1502	22	1569	95.72
MOD	22	32	30	1396	1480	94.32

Table 7. Confusion matrix generated by testing Inception Resnetv2

Class Label	ND	VMD	MD	MOD	Total Data	Accuracy
ND	1608	6	10	5	1629	98.71
VMD	18	1540	30	12	1600	96.25
MD	6	10	1543	10	1569	98.34
MOD	0	8	6	1466	1480	99.04

Table 8. Confusion Matrix generated by testing Resnet50v2

Class Label	ND	VMD	MD	MOD	Total Data	Accuracy
ND	1592	18	10	9	1629	97.72
VMD	8	1580	2	10	1600	98.75
MD	2	6	1559	2	1569	99.36
MOD	0	4	6	1470	1480	99.32

In the above Table 6 and Table 7 showing confusion matrix on testing for Xception and Resnetv2. In the above Table 8, can be observed that Resnet50v2 was successful in classification and appropriately classified. Thus, Resnet50v2's overall testing accuracy was 99.25%. Moreover, other models like VGG16, DenseNet121, Xception, MobileNetV2, and InceptionResNetV2 had good testing accuracy as well, as shown in accordingly. With training and testing accuracy of 99.34% and 99.25%, ResNet50v2 outperforms other models. On the other hand, Resnet50v2 outperformed its competitors with the highest test accuracy and was subsequently selected as the best model for classifying AD. Table 9 shows the comparative results of Alzheimer’s disease.

Table 9. Comparative results of Alzheimer's disease MRI images with different models

Models	Training Accuracy	Testing Accuracy
DenseNet121	89.5	88.5
MobileNetV2	91.4	92.3
VGG16	93.5	94.5
Xception	96.5	93.8
InceptionResNetV2	98.9	98.7
Proposed Model	**99.3**	**99.2**

In particular for categorising MR images, Resnet50v2 is a powerful deep learning model. Figure 7 depicts comparative results of deep learning models. In comparison to other models, Resnet50v2 exhibited with best training and testing accuracy. Inception Resnetv2 achieved the second-highest accuracy rates, outperforming VGG16, DenseNet121, Xception, and MobileNetV2.

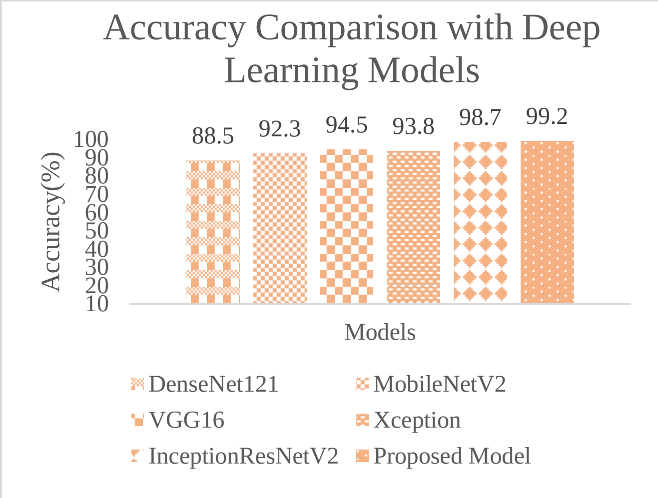

Figure 7. Graphical representation for comparative results of Alzheimer's disease classification

5. CONCLUSIONS

As a result of investigation in this study, it is clear that deep learning is an effective tool for classifying Alzheimer's disease from MRI images. When it comes to making precise decisions based on large, complicated datasets, deep neural networks are undoubtedly very effective. It is therefore apparent that deep learning has a very basic method for solving a problem and producing dynamic findings for the research topic. Deep learning can play a significant role in this process as it can automate the tasks for the neurologists and is not subject to errors caused by humans. In this study, we employed transfer learning to properly categorise MR images into four classes using a variety of deep learning models, including VGG16, DenseNet121, Xception, MobileNetV2, InceptionResNetV2, and Resnet50v2 as the basis model. These models were able to classify the data and had been successfully trained using our datasets. Compare to VGG16, DenseNet121, Xception, MobileNetV2, InceptionResNetV2, and Resnet50v2 models the proposed model had the best training and testing accuracy of model, with 99.34% and 99.25%, respectively. Resnet50v2 with Two phase transfer learning is thus undeniably a successful method for classifying MR images.

REFERENCES

[1] Ghazal, T.M., Issa, G. (2022). Alzheimer disease detection empowered with transfer learning. Computers, Materials & Continua, 70(3): 5005-5019. https://doi.org/10.32604/cmc.2022.020866

[2] Liu, N., Luo, K., Yuan, Z., Chen, Y. (2022). A transfer learning method for detecting alzheimer's disease based on speech and natural language processing. Frontiers in Public Health, 10: 772592. https://doi.org/10.3389/fpubh.2022.772592

[3] Tanveer, M., Rashid, A.H., Ganaie, M.A., Reza, M., Razzak, I., Hua, K.L. (2021). Classification of Alzheimer's disease using ensemble of deep neural networks trained through transfer learning. IEEE Journal of Biomedical and Health Informatics, 26(4): 1453-1463. https://doi.org/10.1109/JBHI.2021.3083274

[4] Khan, R.U., Tanveer, M., Pachori, R.B., Alzheimer's Disease Neuroimaging Initiative (ADNI). (2021). A novel method for the classification of Alzheimer's disease from normal controls using magnetic resonance imaging. Expert Systems, 38(1): e12566. https://doi.org/10.1111/exsy.12566

[5] Raju, M.S.N., Rao, B.S. (2022). Colorectal cancer disease classification and segmentation using a novel deep learning approach. International Journal of Intelligent Engineering Systems, 15(4): 227-236. https://doi.org/10.22266/ijies2022.0831.21

[6] Umbach, G., Kantak, P., Jacobs, J., Kahana, M., Pfeiffer, B.E., Sperling, M., Lega, B. (2020). Time cells in the human hippocampus and entorhinal cortex support episodic memory. Proceedings of the National Academy of Sciences, 117(45): 28463-28474. https://doi.org/10.1073/pnas.2013250117

[7] Nanni, L., Interlenghi, M., Brahnam, S., Salvatore, C., Papa, S., Nemni, R., Castiglioni, I., Alzheimer's Disease Neuroimaging Initiative. (2020). Comparison of transfer learning and conventional machine learning applied to structural brain MRI for the early diagnosis and prognosis of Alzheimer's disease. Frontiers in neurology, 11: 576194. https://doi.org/10.3389/fneur.2020.576194

[8] Prakash, D., Madusanka, N., Bhattacharjee, S., Park, H.G., Kim, C.H., Choi, H.K. (2019). A comparative study of Alzheimer's disease classification using multiple transfer learning models. Journal of Multimedia Information System, 6(4): 209-216. https://doi.org/10.33851/JMIS.2019.6.4.209

[9] Aparna, M., Rao, S.B. (2022). A hybrid siamese-LSTM (Long short-term memory) for classification of Alzheimer's disease. International Journal of Software Innovation (IJSI), 10(1): 1-14. https://doi.org/10.4018/IJSI.309720

[10] Madusanka, N., Choi, H.K., So, J.H., Choi, B.K. (2019). Alzheimer's disease classification based on multi-feature fusion. Current Medical Imaging, 15(2): 161-169. https://doi.org/10.2174/1573405614666181012102626

[11] Xin, M., Wang, Y. (2019). Research on image classification model based on deep convolution neural network. EURASIP Journal on Image and Video Processing, 2019: 1-11. https://doi.org/10.1186/s13640-019-0417-8

[12] Afzal, S., Maqsood, M., Nazir, F., Khan, U., Aadil, F., Awan, K.M., Mehmood, I., Song, O.Y. (2019). A data augmentation-based framework to handle class imbalance problem for Alzheimer's stage detection. IEEE Access, 7: 115528-115539. https://doi.org/10.1109/ACCESS.2019.2932786

[13] Hong, X., Lin, R., Yang, C., Zeng, N., Cai, C., Gou, J., Yang, J. (2019). Predicting Alzheimer's disease using LSTM. Ieee Access, 7: 80893-80901. https://doi.org/10.1109/ACCESS.2019.2919385

[14] El-Dahshan, E.S.A., Hosny, T., Salem, A.B.M. (2010). Hybrid intelligent techniques for MRI brain images classification. Digital Signal Processing, 20(2): 433-441. https://doi.org/10.1016/j.dsp.2009.07.002

[15] Ahmed, S., Choi, K.Y., Lee, J.J., Kim, B.C., Kwon, G.R., Lee, K.H., Jung, H.Y. (2019). Ensembles of patch-based classifiers for diagnosis of Alzheimer diseases. IEEE Access, 7: 73373-73383.

https://doi.org/10.1109/ACCESS.2019.2920011
[16] Islam, J., Zhang, Y. (2017). A novel deep learning based multi-class classification method for Alzheimer's disease detection using brain MRI data. In Brain Informatics: International Conference, BI 2017, Beijing, China, November 16-18, 2017, Proceedings (pp. 213-222). Springer International Publishing. https://doi.org/10.1007/978-3-319-70772-3_20
[17] Zhang, J., Liu, M., An, L., Gao, Y., Shen, D. (2017). Alzheimer's disease diagnosis using landmark-based features from longitudinal structural MR images. IEEE Journal of Biomedical and Health Informatics, 21(6): 1607-1616. https://doi.org/10.1109/JBHI.2017.2704614
[18] Guerrero, R., Wolz, R., Rao, A.W., Rueckert, D., Alzheimer's Disease Neuroimaging Initiative (ADNI. (2014). Manifold population modeling as a neuro-imaging biomarker: application to ADNI and ADNI-GO. NeuroImage, 94: 275-286. https://doi.org/10.1016/j.neuroimage.2014.03.036
[19] Ahmed, O.B., Mizotin, M., Benois-Pineau, J., Allard, M., Catheline, G., Amar, C.B., Alzheimer's Disease Neuroimaging Initiative. (2015). Alzheimer's disease diagnosis on structural MR images using circular harmonic functions descriptors on hippocampus and posterior cingulate cortex. Computerized Medical Imaging and Graphics, 44: 13-25. https://doi.org/10.1016/j.compmedimag.2015.04.007
[20] Ebrahimi-Ghahnavieh, A., Luo, S., Chiong, R. (2019). Transfer learning for Alzheimer's disease detection on MRI images. In 2019 IEEE International Conference on Industry 4.0, Artificial Intelligence, and Communications Technology (IAICT), Bali, Indonesia, pp. 133-138. https://doi.org/10.1109/ICIAICT.2019.8784845
[21] Jin, K.H., McCann, M.T., Froustey, E., Unser, M. (2017). Deep convolutional neural network for inverse problems in imaging. IEEE Transactions on Image Processing, 26(9): 4509-4522. https://doi.org/10.1109/TIP.2017.2713099
[22] Zaabi, M., Smaoui, N., Derbel, H., Hariri, W. (2020). Alzheimer's disease detection using convolutional neural networks and transfer learning based methods. In 2020 17th International Multi-Conference on Systems, Signals & Devices (SSD), Monastir, Tunisia, pp. 939-943. https://doi.org/10.1109/SSD49366.2020.9364155
[23] Abed, M.T., Fatema, U., Nabil, S.A., Alam, M.A., Reza, M.T. (2020). Alzheimer's disease prediction using convolutional neural network models leveraging pre-existing architecture and transfer learning. In 2020 Joint 9th International Conference on Informatics, Electronics & Vision (ICIEV) and 2020 4th International Conference on Imaging, Vision & Pattern Recognition (icIVPR), Kitakyushu, Japan, pp. 1-6. https://doi.org/10.1109/ICIEVicIVPR48672.2020.9306649
[24] Shin, H.C., Roth, H.R., Gao, M., Lu, L., Xu, Z., Nogues, I., Yao, J., Mollura, D., Summers, R.M. (2016). Deep convolutional neural networks for computer-aided detection: CNN architectures, dataset characteristics and transfer learning. IEEE Transactions on Medical Imaging, 35(5): 1285-1298. https://doi.org/10.1109/TMI.2016.2528162
[25] Tajbakhsh, N., Shin, J.Y., Gurudu, S.R., Hurst, R.T., Kendall, C.B., Gotway, M.B., Liang, J. (2016). Convolutional neural networks for medical image analysis: Full training or fine tuning? IEEE Transactions on Medical Imaging, 35(5): 1299-1312. https://doi.org/10.1109/TMI.2016.2535302
[26] Beheshti, I., Demirel, H., Alzheimer's Disease Neuroimaging Initiative. (2016). Feature-ranking-based Alzheimer's disease classification from structural MRI. Magnetic Resonance Imaging, 34(3): 252-263. https://doi.org/10.1016/j.mri.2015.11.009
[27] Yedukondalu, J., Sharma, L.D. (2023). Cognitive load detection using circulant singular spectrum analysis and Binary Harris Hawks Optimization based feature selection. Biomedical Signal Processing and Control, 79: 104006. https://doi.org/10.1016/j.bspc.2022.104006
[28] Moradi, E., Pepe, A., Gaser, C., Huttunen, H., Tohka, J., Alzheimer's Disease Neuroimaging Initiative. (2015). Machine learning framework for early MRI-based Alzheimer's conversion prediction in MCI subjects. Neuroimage, 104: 398-412. https://doi.org/10.1016/j.neuroimage.2014.10.002
[29] Rajeswari, S.S., Nair, M. (2021). A Transfer Learning Approach for Predicting Alzheimer's Disease. In 2021 4th Biennial International Conference on Nascent Technologies in Engineering (ICNTE), NaviMumbai, India, pp.1-5. https://doi.org/10.1109/ICNTE51185.2021.9487746
[30] Khan, N.M., Abraham, N., Hon, M. (2019). Transfer learning with intelligent training data selection for prediction of Alzheimer's disease. IEEE Access, 7: 72726-72735. https://doi.org/10.1109/ACCESS.2019.2920448
[31] Raju, M.S.N., Rao, B.S. (2022). Classification of colon and lung cancer through analysis of histopathology images using deep learning models. Ingénierie des Systèmes d'Information, 27(6): 967-971. https://doi.org/10.18280/isi.270613
[32] Gollapalli, M., Kudos, S.A., Alhamad, M.A., Alshehri, A.A., Alyemni, H.S., Alali, M.O., Mohammad, R.M.A., Khan, M.A.A., Abdulqader, M.M., Aloup, K.M. (2022). Machine learning models towards prediction of COVID and Non-COVID 19 patients in the hospital's intensive care units (ICU). Mathematical Modelling of Engineering Problems, 9(6): 1741-1780. http://dx.doi.org/10.18280/mmep.090605
[33] Kateb, Y., Meglouli, H., Khebli, A. (2023). Coronavirus diagnosis based on chest x-ray images and pre-trained DenseNet-121. Revue d'Intelligence Artificielle, 37(1): 23-28. https://doi.org/10.18280/ria.370104